Catalysis Today 151 (2010) 291–303

Contents lists available at ScienceDirect

Catalysis Today

journal homepage: www.elsevier.com/locate/cattod

'Fast' NOx storage on Pt/BaO/γ-Al_2O_3 Lean NOx Traps with $NO_2 + O_2$ and $NO + O_2$: Effects of Pt, Ba loading

Saurabh S. Chaugule[a], Aleksey Yezerets[b], Neal W. Currier[b], Fabio H. Ribeiro[a], W. Nicholas Delgass[a,*]

[a] School of Chemical Engineering, Purdue University, 480 Stadium Mall Drive, West Lafayette, IN 47907-2100, United States
[b] Cummins Inc., 1900 McKinley Ave, Columbus, IN 47201, United States

ARTICLE INFO

Article history:
Available online 15 March 2010

Keywords:
NOx storage
Pt–Ba interaction
Pt dispersion
Barium
Lean NOx Trap (LNT)
Integral reactor

ABSTRACT

NOx storage on Pt/BaO/γ-Al_2O_3 Lean NOx Traps (LNTs) has been studied with a particular focus on the NOx storage capacity (NSC) of these traps for the time up to which 1% of the inlet [NOx] escapes the trap. This complete or 'fast' NOx sorption capability of LNTs for appreciable amounts of time is what makes these catalysts useful for automotive NOx emission abatement. The fast NSC for LNT formulations with combinations of a range of Pt (0.6–6.3 wt.%) and Ba (4–20 wt.%) loadings was measured under various lean feed compositions including NO, NO_2 and $NO + NO_2$ as the NOx sources and presence and absence of 7%CO_2 and 7%H_2O. All the measurements were performed at 300 °C and at a space velocity of 30,000 h^{-1}. The complex trends in the fast NSC due to various Pt, Ba loading combinations are explained with the help of a phenomenological model. The model addresses the trends in fast NSC primarily through combinations of NOx storage contributions in parallel pathways on Ba vicinal to Pt and Ba uninfluenced by Pt. We attribute the influence of Pt to the spillover of dissociated oxygen atoms from Pt to the vicinal Ba sites. This Pt–Ba synergy was found to play a dominating role in governing the fast NSCs of all the LNT samples especially in presence of CO_2, H_2O and $CO_2 + H_2O$ in the lean feed. It was also found to be the prominent factor in limiting the fast NSC when NO and $NO + NO_2$ (with low NO_2/NO) were the NOx sources rather than NO_2. We propose that the NOx storage process on Ba vicinal to Pt involves a localized reaction front of NOx that travels through the catalyst bed with saturation of those sites. This process has no preference between NO and NO_2 as a precursor. CO_2 and H_2O affect through competition for both types of Ba sites available for NOx storage.

1. Introduction

Lean NOx Trap (LNT) technology also known as NOx Storage–Reduction catalysis (NSR) or NOx Absorber Catalysis (NAC) is a frontrunner in those being investigated for the NOx emission abatement from the automotive lean burn gasoline and diesel engine exhaust [1,2]. The traditional three way catalysts (TWCs) are tuned to give excellent NOx conversion when the engine runs at a stoichiometric air to fuel (A/F) ratio of about 14.6/1 on a weight basis, but they cannot reduce NOx under excess O_2 in the exhaust when the engine runs leaner in fuel at 25/1 [3]. This challenge led to the development of multicomponent LNT catalysts to eliminate the shortcoming of the traditional TWCs [4]. Lean NOx traps are composed of at least three components, a high surface area support like γ-Al_2O_3, an alkali metal (*e.g.* Na, K) or alkaline earth metal (*e.g.* Ba, Mg) as the NOx storage component and a precious metal (*e.g.* Pt, Pd, Rh) as the redox component [1,4,5]. In the literature, Pt/BaO/Al_2O_3 containing model LNTs are the most studied [1]. Since a finite amount of Ba has a finite NOx storage capacity, it needs to be regenerated periodically. Therefore the LNTs operate in a cyclic fashion with alternate fuel lean and fuel rich phases. During the lean phase NO oxidizes to NO_2 on Pt and NOx ($NO + NO_2$) is stored on Ba in the form of nitrites or nitrates [1,6–10]. Before unacceptable amounts of NOx start escaping the LNT, the engine has to switch from lean to rich operating conditions. Then, in presence of reductants such as CO, H_2 and unburned hydrocarbons, NOx is released from Ba and reduced on Pt to form primarily N_2 and H_2O [1,11,12].

Our ultimate objective is to be able to understand all these processes in enough detail to facilitate the building of a robust predictive mathematical model of the process for any given lean/rich feed condition and LNT composition. In our laboratory we have previously studied the regeneration of these Pt/BaO/γ-Al_2O_3 LNTs with H_2 as a model reductant and found that the regeneration occurs through a plug flow mechanism [11] involving a localized reaction front. Ammonia was found out to be the intermediate during reduction of stored NOx with H_2. Furthermore, the regeneration process

* Corresponding author at: School of Chemical Engineering, Purdue University, Forney Hall of Chemical Engineering, 480 Stadium Mall Drive, West Lafayette, IN 47907-2100, United States. Tel.: +1 765 494 4059; fax: +1 765 494 0805.
E-mail address: delgass@purdue.edu (W.N. Delgass).

0920-5861/$ – see front matter © 2010 Elsevier B.V. All rights reserved.
doi:10.1016/j.cattod.2010.02.024

was found to be limited only by supply of hydrogen atoms from H_2 or NH_3 and was not affected by presence of CO_2 and H_2O in the range of 200–300 °C [12]. Cao et al. [13] successfully utilized these insights to model the experimentally observed time dependent exit concentration profiles of N_2, H_2O and NH_3 in the effluent and the temperature profiles generated by the exothermic reduction reactions during the regeneration of the LNT. The mechanism of NO oxidation on Pt has also been investigated in our laboratory by Mulla et al. [14–16] and it has been found that the turnover rate (TOR) for NO oxidation is first order in NO and O_2 while NO_2 is an inhibitor with an inverse first order dependence on the TOR. These experimental insights have also been used to model the coupled NO oxidation and NOx storage process by Cao et al. [13] and Kromer et al. [17]. In both papers [13,17], NOx storage was tracked for a given lean phase exposure time by modeling the NOx breakthrough profile, *i.e.* the exit NOx concentration vs. time recorded during exposure of a LNT to the lean phase feed. Based on the preliminary NOx storage studies on a 2.1 wt.%Pt/20 wt.%Ba/Al_2O_3 containing LNT sample in our laboratory, two NOx storage models, both being able to account for the asymmetric nature of the NOx breakthrough profiles, were proposed [13,17]. In the first, two sites in a parallel model could fit the NOx breakthrough data using two separate time constants for distinct NOx storage reaction pathways on Ba vicinal to Pt and Ba far from, or uninfluenced by, Pt. In the second model, a two sites in series model could fit the same data with two time constants for NOx storage on surface Ba sites and on bulk Ba sites reached only by diffusion through large particles. At that point our experimental data was not sufficient to distinguish whether one of the two scenarios or a combination of them was the best description of the phenomena. Also the NOx storage model was not mature enough to address the variation with NO or NO_2 as the NOx source and effects of CO_2 and H_2O on NOx storage on LNT samples containing different Pt, Ba loadings.

NOx storage trends and mechanisms have been investigated in great detail using various techniques by several contemporary research groups on different catalyst formulations and under various feed compositions and reaction conditions. The coupled NO oxidation and NOx sorption processes, uniqueness of catalyst formulation and preparation methods, sensitivity of the reaction pathways to reaction conditions, pretreatment protocols, NOx storage testing protocols, intimate dependence on regeneration steps prior to NOx storage have produced a variety of at times contradicting results. The complexity arising out of efforts to integrate these results into a comprehensive description of the process still fuels the debate about balancing the exact physicochemical nature of the NOx sorption/storage process and the detail that is necessary to build a robust predictive mathematical model of the process useful for the practical/commercial application of the LNTs. Here we discuss in brief the pertinent results and hypotheses/arguments made to justify them.

There is a consensus in the literature that improved NO oxidation to NO_2 results in improved NOx storage performance [1,18,19] and that NO_2 is the precursor for the storage process on Ba [7,20–31]. The lower NOx storage capacity with $NO + O_2$ vs. $NO_2 + O_2$ is attributed to the Ba sites near the monolith inlet being underutilized due to inadequate supply of NO_2 [18] due to the integral nature of the monolith channel. The rise in NOx storage capacity with increasing temperature is believed to be due to enhanced NO oxidation [31–36] and the drop after peaking in the range of 300–400 °C is believed to be due to decrease in thermodynamic stability of the nitrate species [31,35–37]. The overall NOx storage behavior with temperature when NO is the NOx source is thus volcano shaped. Even when the NO oxidation limitation is eliminated by using NO_2 as the NOx source, the volcano profile is retained [31] highlighting the underlying effect of temperature on NOx storage kinetics and thermodynamic stability of adsorbed species. Minor amounts of NOx storage on γ-Al_2O_3 compared to the BaO component have also been reported [8,10,38,39].

$Ba(NO_3)_2$ species have been consistently observed on Pt/BaO/Al_2O_3 at higher temperatures using various techniques while $Ba(NO_2)_2$ has been observed at lower temperatures (150–200 °C) [1,4,21,30,31,34,40–42] and the possibility that the nitrite species is the precursor to nitrate at higher temperatures has been used in various models used to describe the NOx storage process [1]. It has been proposed in a number of studies that this nitrate formation in the presence of NO or NO_2 and O_2 in the feed can occur on Ba vicinal to Pt using the dissociated oxygen adatoms on Pt [1,24,28,31,34,36,37,43,44]. Since such sites are limited, when they saturate, their role in NOx storage diminishes [43]. The presence of such Ba sites vicinal to Pt and their advantage for NOx storage has been investigated by studying NOx storage on Pt/Al_2O_3–BaO/Al_2O_3 mechanical mixtures vs. that on Pt/BaO/Al_2O_3 with the conclusion that the enhancing effect of Pt on NOx storage is observed only in the later case, possibly due to shorter length scales involved for surface diffusion of dissociated oxygen adatoms [22,45,46]. At long storage times, the NO_2 disproportionation mechanism is believed to be dominant, during which NO_2 can directly adsorb on Ba not vicinal to Pt via a sequence of steps in which one NO molecule is evolved for every three NO_2 molecules adsorbed. The oxidant in this mechanism is NO_2 [1,23,24,27,47].

A shrinking core model has been used in several studies [17,23,48–50] to account for diffusion of the NOx species inside large Ba particles on samples with relatively high Ba loading. Recently, using ultra-high-field solid-state MAS ^{27}Al-NMR, Kwak et al. [51,52] have shown that penta-coordinated Al^{3+} sites are the preferential nucleation sites for BaO on γ-Al_2O_3 and that at 4 and 8 wt.%. Ba loading, BaO monomers and dimers are formed on the alumina surface on samples prepared by the incipient wetness method. More recently Lindholm et al. [53] have shown that the NOx storage capacity depends on the method of preparation of the catalyst, particularly the Pt, Ba deposition sequence and Corbos et al. [54] have reported that the pretreatment conditions in addition to the method of preparation also have an effect on NOx storage. Works by Clayton et al. [19] and Al-Harbi et al. [18] highlight the impact of Pt dispersion on NOx storage. All these results indicate that the morphologies of the Pt and Ba phases lead to formation of different types of sorption sites and affect the NOx storage capacity on the Pt/BaO/γ-Al_2O_3 LNTs.

Quantification of those effects is difficult since the Ba morphology on the surface is sensitive to reaction conditions and feed compositions. Szanyi et al. [55,56] have reported such changes during NO_2 storage and regeneration caused by the presence of H_2O in the feed. Under realistic conditions, the lean feed always contains CO_2 in addition to H_2O. It has been shown that at temperatures as high as 360 °C, $BaCO_3$ and $Ba(OH)_2$ coexist on the surface [32,57]. There is no doubt in the LNT research community that in presence of CO_2 and H_2O in the gas phase feed there is a combination of carbonate, carboxylate and hydroxyl species on the surface which are the precursors for nitrite/nitrate species during NOx storage. The thermodynamic competition for trapping sites and kinetic factors affect the availability of Ba sites for NOx storage [1]. However the dynamics of these processes are not well quantified since multiple parameters affect the system, making interpretation of the data difficult.

2. Experimental methods

2.1. Catalyst samples

The series of seven Pt/Ba/γ-Al_2O_3 Lean NOx Trap catalysts used in this study were supplied by Johnson Matthey, Plc. They contained

Table 1
Fraction of Pt exposed (E_{Pt}) on fresh and de-greened Pt/BaO/γ-Al_2O_3 samples.

Sample	[a]E_{Pt} (fresh sample) (% ± 3)	[a]E_{Pt} (de-greened sample) (% ± 3)
6.3Pt/20Ba	37	21
2.1Pt/20Ba	31	19
0.7Pt/20Ba	26	19
1.9Pt/8Ba	58	50
5.3Pt/4Ba	57	50
1.8Pt/4Ba	65	60
0.6Pt/4Ba	66	62

[a] E_{Pt} = [number of surface Pt atoms/total number of Pt atoms × 100], fraction of Pt exposed measured by CO titration (Section 2.4).

different combinations of Pt and Ba loadings as listed in Table 1. Pt and Ba loadings were measured and provided to us by the manufacturer. Each sample is referred to as *m*Pt/*n*Ba, where *m* and *n* correspond to the wt.% of Pt and Ba loading of the γ-Al_2O_3 deposited on the cordierite monolith. In the text, we have referred to various Pt and Ba loadings as *m*%Pt and *n*%Ba, respectively. The monoliths had a cell density of 400 cpsi (cells in.$^{-2}$). The component deposition sequence on the cordierite monolith substrate was γ-Al_2O_3 washcoat followed by Pt and then Ba. These seven samples can be categorized into three groups: (1) 20%Ba samples with three different Pt loadings, (2) 4%Ba samples with three different Pt loadings and (3) samples with *ca.* 2%Pt and three different Ba loadings. Cylindrical cores measuring 3 in. in length and *ca.* 0.65 in. in diameter were cut from the monolith samples provided. The washcoat loading (g in.$^{-3}$) on each monolith was slightly different and as a result, equal volume cores of 20%Ba and 4%Ba samples with comparable Pt loading (*e.g.* 6.3Pt/20Ba and 5.3Pt/4Ba) used in this study actually contained similar amounts of Pt (Table 2). For to the same reason, the amount of Ba on different monolith cores with same *n* varies slightly (Table 2).

2.2. Flow reactor setup

The NOx storage and reduction experiments were performed in a bench-top tubular stainless steel reactor. The catalyst core was wrapped in high-temperature Zetex® insulation and inserted into the reactor tube. The insulation matting sealed the space between the cylindrical monolith core and the reactor wall, minimizing gas bypass around the sample. A 3 in. long plug of small quartz beads of *ca.* 3 mm dia., held in place by circular pieces of stainless steel wire mesh, was placed upstream of the catalyst sample in the reactor tube to ensure mixing and uniformity of the gas flow. The quartz beads also acted as a thermal mass facilitating heat transfer from the reactor wall to the gas mixture being fed. The reactor tube was placed inside a temperature controlled tube furnace. Two K type thermocouples, aligned with the axis of the reactor tube, were placed 5 mm upstream and 5 mm downstream of the monolith core to measure the inlet and outlet gas temperatures. To maintain uniform catalyst temperature across the length of the core, the inlet gas was preheated by passing it through a pre-heater assembly consisting of a helical coil *ca.* 3 in. diameter, made out of 0.25 in. diameter stainless steel tubing, and placed inside a temperature controlled hollow cylindrical Watlow® ceramic fiber heater. The specialty gas mixtures (3.5%NO/Ar, 5%NO_2/Ar) were from Praxair. Argon (99.997%) was used as the inert carrier gas. The gas flow rates were controlled using a bank of Brooks 5850C series mass flow controllers. For experiments containing water in the feed, deionized water was added to the inert carrier gas stream by using a shell side temperature controlled Perma Pure MH-070 series humidifier. The stainless steel tubing downstream of the humidifier was heated to *ca.* 120 °C with a heating tape, to avoid water condensation. A 3-way valve was used to direct the inert carrier gas flow through either the humidifier or tubing bypassing the humidifier to choose between wet and dry feed conditions respectively. Precaution was taken to minimize the dead volume while connecting reactant gas feeder lines to the inert carrier gas line. The O_2 feed line was connected to the carrier gas line downstream of the NO feed line connection to avoid NO oxidation in the feed line by exposure to the oxygen rich carrier gas stream before the NO reached the catalyst. Various feed compositions and fast lean-rich switching were achieved by using LabVIEW™ controlled 2-way and 3-way valves installed downstream of the mass flow controllers.

The effluent gases from the reactor were analyzed by an MKS MultiGas™ 2030 gas phase FT-IR spectrometer. Utilizing the vendor supplied calibration files the spectrometer was used to monitor and record the NO, NO_2, N_2O, NH_3, CO_2 and H_2O concentrations in the effluent with time at 0.95 s resolution. N_2 in the effluent was detected using SRS RGA 200, a quadrupole mass spectrometer. The mass spectrometer was calibrated to measure N_2 concentrations in the 0–6000 ppm range by sampling calibrated N_2/Ar mixtures. Argon was used as the inert carrier gas to allow the measurement of released N_2 during LNT regeneration. The feed composition at reactor inlet was analyzed by directing the feed flow to bypass the reactor. All the effluent gas lines were heated to *ca.* 120 °C using heating tapes to avoid water condensation inside the tubing.

2.3. Catalyst de-greening

All fresh or 'green' LNT catalyst cores were pretreated in the flow reactor system to achieve reproducible NOx storage–reduction performance during testing over long intervals of time. We refer to our pretreatment procedure as 'de-greening'. It follows a two-step protocol comprized of treatments at 600 and 300 °C. During high-temperature treatment, short lean (54 s) and rich (6 s) cycles were run for 1.5 h at 600 °C and GHSV of 30,000 h^{-1}. The lean phase feed during this step contained 300 ppm NO + 10%O_2 + 7%CO_2 + 8%H_2O in Ar and rich phase feed consisted of 2.45%H_2 + 7%CO_2 + 8%H_2O in Ar. After the 90 redox cycles at 600 °C, the catalyst sample was cooled to 300 °C in Ar at 30,000 h^{-1}. Then during the low temperature treatment, at least three long lean (1 h) and rich (10 min) cycles were run at 300 °C, the feed composition and GHSV remaining the same as that for the high treatment step. The de-greened LNT catalyst samples were found to give reproducible NOx storage capacities and NOx breakthrough profiles after numerous cycles at 300 °C with various lean, rich feed compositions in random order

Table 2
Pt/BaO/γ-Al_2O_3 samples with total amounts of Pt and Ba on monolith cores (3 in. length, 0.65 in. dia.) used for NOx storage experiments, fractions of Pt exposed after de-greening and exposed Pt/Ba ratios.

Sample	Pt on sample (μmol)	E_{Pt} (% ± 3)	Exposed Pt (μmol)	Ba on sample (μmol)	Exposed Pt/Ba
6.3Pt/20Ba	372	21	78 ± 11	1680	0.046
2.1Pt/20Ba	124	19	24 ± 4	1680	0.014
0.7Pt/20Ba	40	19	8 ± 1	1650	0.005
1.9Pt/8Ba	124	50	62 ± 4	751	0.083
5.3Pt/4Ba	372	50	186 ± 11	397	0.467
1.8Pt/4Ba	124	60	74 ± 4	394	0.190
0.6Pt/4Ba	40	62	25 ± 1	383	0.065

and even after unloading–reloading the catalyst cores in the flow reactor. The 600 °C de-greening step was inspired by recent work by Adams et al. [58] and Epling et al. [59] but the 300 °C step was found to be necessary to ensure reproducible NSR performance over repeated testing after 3–6 month long intervals. Also, using two separate fresh 2.1Pt/20Ba cores from the same source monolith, we observed that the sequence in which the de-greening steps are performed does not affect the performance on the de-greened samples.

2.4. Fraction of Pt exposed measurement by CO titration

Fraction of Pt exposed (E_{Pt}) is defined as the ratio of surface Pt atoms to total number of Pt atoms present and expressed as a percentage. To measure the number of surface Pt atoms on the Pt/BaO/γ-Al_2O_3 catalysts we used a CO titration method. First, the NOx storage capacity of a regenerated trap was saturated by flowing 300 ppm NO_2 + 10%O_2 + 7%CO_2 + 7%H_2O in Ar for 1.5 h at 300 °C, 30,000 h^{-1}. Then NO_2, O_2, CO_2 and H_2O were turned off and the system was purged with Ar at the same space velocity for about 20 min while cooling the sample to 150 °C. During this process, the reactant gases were flushed out of the reactor, leaving behind the chemisorbed oxygen on Pt while the barium phase participating in NOx sorption was converted primarily to barium nitrate and some to barium carbonate or carboxylate depending on the Ba loading on the sample under consideration. This step was essential to ensure that only the oxygen atoms chemisorbed on Pt would contribute to the CO titration step, which consisted of flowing 1.5%CO in Ar at 15,000 h^{-1} while maintaining the temperature at 150 °C and recording the CO_2 peak produced by oxidation of CO by oxygen atoms adsorbed on Pt. The GHSV was adjusted to obtain a well-defined peak, as the amount of CO_2 produced during titration of the Pt surface was small. The amount of CO_2 was quantified by integrating the area under the CO_2 peak and using the known concentration of CO and total volumetric flow rate of the feed. This amount of CO_2 in μmol equals the amount of surface Pt in μmol, assuming that one oxygen atom is adsorbed on each surface Pt atom [60,61], which results in production of one CO_2 molecule from CO. The fractions of Pt exposed calculated using these CO titration experiments before and after de-greening are reported in Table 1. The fractions of Pt exposed calculated by this method for the fresh samples (before de-greening) were within ±3% with those reported by Cumaranatunge [62] using the H_2–O_2 titration method [60] to measure surface Pt on the scraped washcoats from fresh samples. Those samples were obtained from the same source monolith from which the cylindrical cores used in this study were cut.

2.5. NOx storage experiments

At least three lean (7 min)–rich (4 min) conditioning cycles were performed prior to the long NOx lean (storage for 1–1.5 h)–rich (regeneration for 15 min) cycle from which the NOx storage capacity (NSC) reported in this work was calculated. The lean and rich feed compositions for the conditioning cycles were kept the same as the feed under which the NSC measurements were made. For example, to measure the NSC of the LNT under NO + O_2 + CO_2 environment, the lean phase feed contained 300 ppm NO + 10%O_2 + 7%CO_2 in Ar and the rich phase feed contained 1%H_2 + 7%CO_2 in Ar for all four cycles. This was done in order to achieve a cyclic steady-state as the NOx storage behavior on Pt/BaO/γ-Al_2O_3 catalysts depends on the chemical state of the Ba phase at the beginning of NOx storage. All the experiments were performed at 300 °C and 30,000 h^{-1} with combinations of 300 ppm NO or NO_2 + 10%O_2 in Ar with 7%CO_2, 7%H_2O and 7%CO_2 + 7%H_2O in the lean feed. The NOx storage capacity was also measured using experiments in which lean feed contained mixtures of 50–650 ppm NO + 300 ppm NO_2 + 10%O_2 in Ar in presence and absence of 7%CO_2 + 7%H_2O at 300 °C, 30,000 h^{-1}. The nitrogen balance between the amount of NOx stored during lean phase and nitrogen containing species in the effluent recorded during the rich phase was found to agree within 5% of each other for both short and long cycles. To confirm complete regeneration, separate experiments were performed in which the temperature was ramped to 450 °C after short and long lean–rich cycles similar in time periods to those during NOx storage experiments. No nitrogen containing species were detected in the effluent during the temperature ramp. Thus, we ensured that the entire amount of Ba participating in the NOx sorption or storage process was regenerated prior to the switch from rich to lean phase feed.

2.6. 'Fast' NOx storage measurements

The NOx storage capacity or NSC (μmol) for a given period of lean phase exposure, t_S (s) is calculated as

$$NSC_{t_s} = \alpha \cdot \int_0^{t_s} [C^0_{NOx} - C_{NOx}(t)]dt \quad (1)$$

where C^0_{NOx} is the inlet NOx concentration (ppm) and $C_{NOx}(t)$ is the NOx concentration (ppm) in the effluent at any time t (s) recorded by the FT-IR in our case. The constant α (μmol/ppm s) converts the NSC_{ts} from units of ppm s to μmol.

The property that makes application of these Pt/BaO/γ-Al_2O_3 LNTs for NOx abatement so promising is their ability to completely capture NOx from the exhaust gas mixture for a short period of time after they are regenerated. We define 'fast' NOx storage as the NOx sorption process occurring on the trap during this short period of time, t_{Sf}. Specifically, we choose t_{Sf} as the time elapsed between the rich to lean feed switch and the instant the NOx slip reaches 1% of the inlet NOx concentration (C^0_{NOx}) level, in other words, when the NOx breakthrough just begins. Then Eq. (1) simplifies to

$$fast\ NSC_{t_{sf}} = \alpha \cdot \int_0^{t_{sf}} [C^0_{NOx} - 0]dt$$
$$\therefore fast\ NSC_{t_{sf}} = \alpha \cdot C^0_{NOx} \cdot t_{sf} \quad (2)$$

which is the area of a rectangle on C_{NOx} vs. t plot. We choose this particular time period because it allows us to eliminate the dependence of the fast NSC of the LNT on the slope of the NOx breakthrough curve resulting from slower NOx storage pathways. Moreover, during practical application of LNTs, if complete elimination of NOx from the exhaust is desired, t_{Sf} as defined here represents the maximum time interval between two rich feed pulses capable of regenerating the Ba phase participating in fast NOx storage.

3. Results

3.1. Fraction of Pt exposed on Pt/BaO/γ-Al_2O_3 LNTs

Table 1 summarizes the fractions of Pt exposed (E_{Pt}) on the series of seven fresh and de-greened Pt/BaO/γ-Al_2O_3 samples measured by CO titration experiments as described in detail in Section 2.4. On all fresh samples with 20%Ba the E_{Pt} is approximately half of that on fresh samples containing 8Ba and 4Ba. As the Pt loading increases on samples with 20%Ba, the E_{Pt} also increased. After the de-greening treatment, the fraction of Pt exposed on all samples containing 20%Ba dropped to about 20%. The drop in E_{Pt} due to de-greening was the highest for 6.3Pt/20Ba (*ca.* 16%) and the lowest for 0.7Pt/20Ba (*ca.* 7%). All other samples, with 8%Ba and 4%Ba, showed a drop of 7–8% in E_{Pt} due to the de-greening treatments. The absolute amounts of Pt and Ba on each of the monolithic cores used for NOx storage experiments (Table 2) were computed with

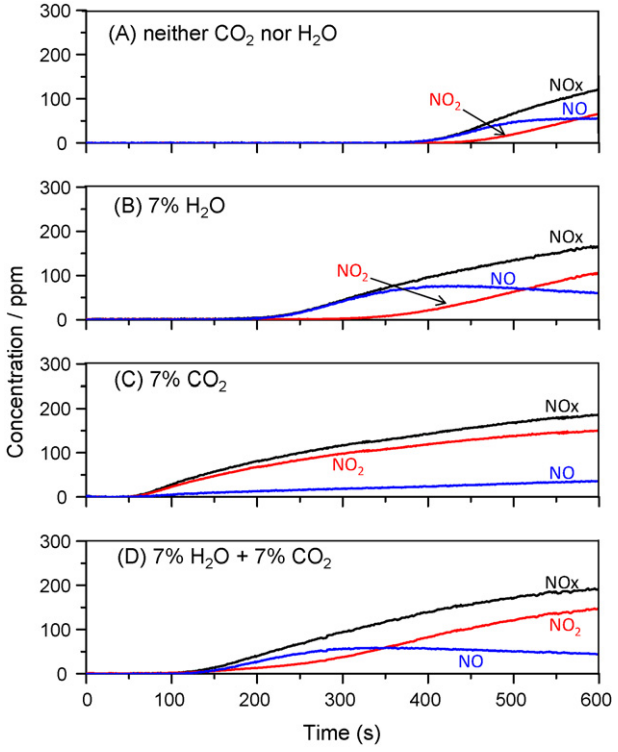

Fig. 1. NO, NO_2 and NOx ($NO+NO_2$) breakthrough profiles for 10 min of NOx storage on 2.1Pt/20Ba at 300 °C, 30,000 h^{-1} with lean feed consisting of 300 ppm NO_2 + 10%O_2 + balance Ar and (A) neither CO_2 nor H_2O, (B) 7%H_2O, (C) 7%CO_2, and (D) 7%H_2O + 7%CO_2.

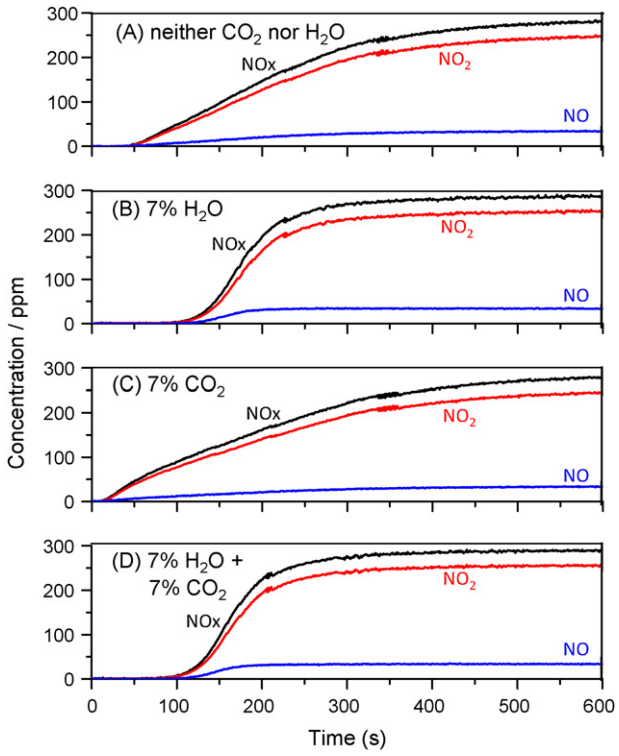

Fig. 2. NO, NO_2 and NOx ($NO+NO_2$) breakthrough profiles for 10 min of NOx storage on 1.9Pt/8Ba at 300 °C, 30,000 h^{-1} with lean feed consisting of 300 ppm NO_2 + 10%O_2 + balance Ar and (A) neither CO_2 nor H_2O, (B) 7%H_2O, (C) 7%CO_2, and (D) 7%H_2O + 7%CO_2.

the knowledge of the weight loading of Pt on the γ-Al_2O_3 washcoat and the washcoat loading on the monolith (g $in.^{-3}$). Using the fraction of Pt exposed after de-greening and the total amount of Pt on the sample, the amount of exposed Pt was then computed (Table 2). Note that the amounts of exposed Pt on 20%Ba samples are 30–60% lower than those for the corresponding samples with 8%Ba and 4%Ba having equal amounts of total Pt.

3.2. *'Fast' NOx storage with $NO_2 + O_2$*

Representative NO, NO_2 and NOx ($NO+NO_2$) breakthrough profiles for samples containing *ca.* 2%Pt and 20%, 8% and 4%Ba are shown in Figs. 1–3, respectively. Lean feed for these experiments consisted of 300 ppm NO_2 + 10%O_2 in Ar with (A) neither CO_2 nor H_2O, (B) 7%H_2O, (C) 7%CO_2, (D) 7%H_2O + 7%CO_2 at 300 °C, 30,000 h^{-1}. Four different NOx breakthrough profiles in each of Figs. 1–3 are labeled to represent the lean feed composition. Our objective is to track the effect of Pt on fast NOx storage on the Ba phase of samples having different Pt, Ba loadings. Here, the choice of NO_2 as the NOx source instead of NO eliminates the primary role of Pt in NOx storage through NO oxidation to NO_2.

Fig. 4 shows the result of a simulation of steady-state NO oxidation on monolithic Pt/γ-Al_2O_3 catalyst, based on prior work published by our research group [13,16,17]. It shows that on a 2Pt/γ-Al_2O_3 (E_{Pt} = 19%) monolith core identical to the 2.1Pt/20Ba sample used in the experiments but without any Ba, at 300 °C, 30,000 h^{-1} with 300 ppm NO_2 + 10%O_2 in Ar, there will be NO production due to the NO_2 decomposition reaction on Pt along the length of a monolith channel. This is attributed to the nature of NO oxidation kinetics in which NO_2 acts as an inhibitor. At the outlet of the 3 in. long monolith channel the NO_2 conversion is *ca.* 6% with the said feed composition. Thus, if Ba present on the LNT samples with similar Pt loadings were to saturate due to NOx storage, the

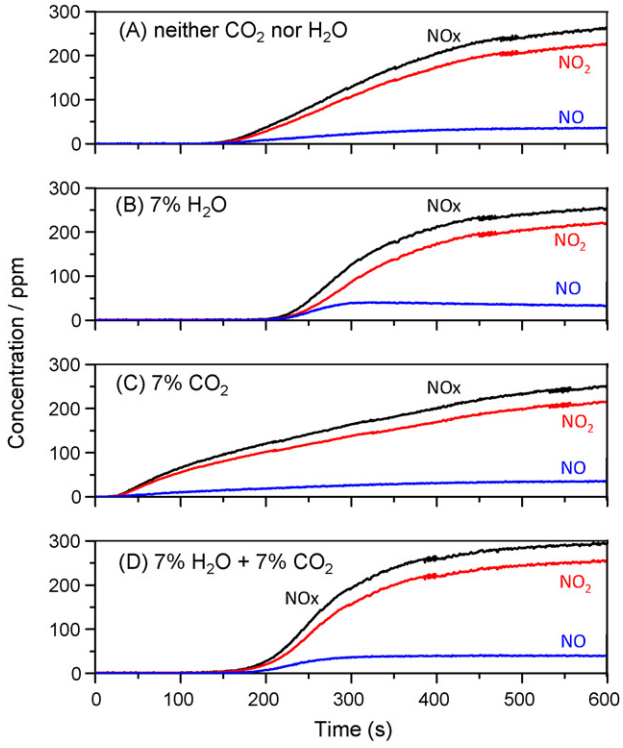

Fig. 3. NO, NO_2 and NOx ($NO+NO_2$) breakthrough profiles for 10 min of NOx storage on 1.8Pt/4Ba at 300 °C, 30,000 h^{-1} with lean feed consisting of 300 ppm NO_2 + 10%O_2 + balance Ar and (A) neither CO_2 nor H_2O, (B) 7%H_2O, (C) 7%CO_2, and (D) 7%H_2O + 7%CO_2.

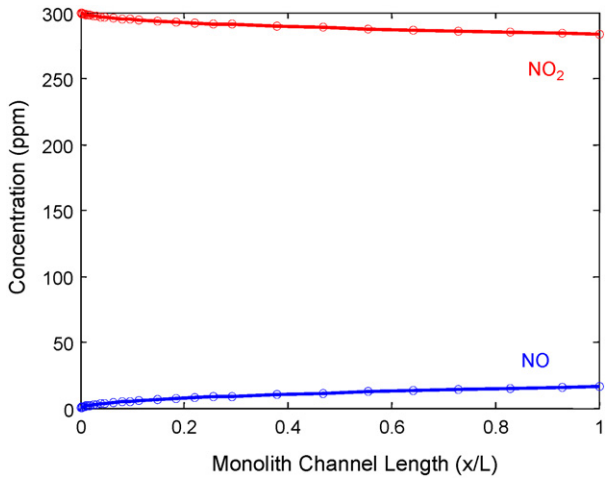

Fig. 4. Simulation result for steady-state NO_2 decomposition along length of a monolith channel, with 300 ppm NO_2 + 10%O_2 + Ar on 2Pt/γ-Al_2O_3 (E_{Pt} = 19%) at 300 °C and 30,000 h^{-1}, leading to NO buildup along the length of the integral reactor.

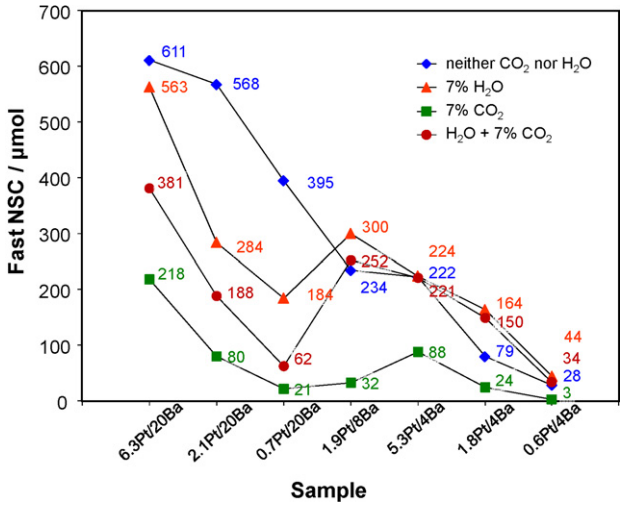

Fig. 5. Fast NOx storage capacity on sample (±10 µmol) at 300 °C, 30,000 h^{-1} with lean feed consisting of 300 ppm NO_2 + 10%O_2 in Ar and neither CO_2 nor H_2O, 7%H_2O, 7%CO_2, 7%H_2O + 7%CO_2.

NO concentration in the effluent would approach 18 ppm at steady-state. Similarly, for 2Pt/γ-Al_2O_3 with E_{Pt} = 50% (corresponding to 1.9Pt/8Ba) and 60% (corresponding to 1.8Pt/4Ba) the simulated NO concentrations at the channel outlet due to NO_2 decomposition are 25 and 27 ppm, respectively. This is consistent with the fact that as the amount of exposed Pt increases, the NO conversion to NO_2 also increases.

Careful analysis of the NO breakthrough profiles for 2.1Pt/20Ba in Fig. 1A–D shows that under different lean feed compositions, as soon as the fast NOx storage phase ended, the effluent NO concentration did not reach the expected 18 ppm level governed by NO_2 decomposition. Under respective feed conditions for Fig. 1A, B and D the effluent NO concentration overshoots the 18 ppm level and then starts decreasing slowly towards it. While in presence of CO_2 for Fig. 1C, the approach of the NO concentration to the maximum and subsequently approaching the expected 18 ppm level due to NO_2 decomposition is much slower. A similar trend in NO breakthrough as with CO_2 (Fig. 1C) was observed across all feed compositions on samples with 8%Ba and 4%Ba (presented in Figs. 2A–D and 3A–D). Moreover, for 2.1Pt/20Ba, Fig. 1A and B show that the NOx breakthrough is driven by NO, while it was observed in Fig. 1C and D that the NO_2 breakthrough precedes that of NO. Also, note that the time at which the NOx breakthrough reaches 3 ppm (*i.e.* 1% of inlet NOx concentration, t_{Sf}) is the longest without CO_2 and H_2O in lean feed. The value of t_{Sf} decreased for the lean feed containing H_2O (Fig. 1B) and decreased even more for lean feed with CO_2 + H_2O (Fig. 1D). It was the lowest for lean feed containing CO_2 (Fig. 1C) on 2.1Pt/20Ba, the highest Ba loading sample we have. The fast NSCs on all the 20%Ba samples corresponding to different lean feed compositions are reported in Fig. 5. Results from Fig. 5 show that effects of respective lean feed composition on fast NSC of 6.3Pt/20Ba and 0.7Pt/20Ba were similar to those seen on 2.1Pt/20Ba.

On samples with 1.9Pt/8Ba and 1.8Pt/4Ba, depending on the lean feed composition, NO_2 and NO breakthrough occurred either simultaneously or NO_2 breakthrough preceded NO by a few seconds (Figs. 2A–D and 3A–D) but in none of the cases did we observe NO breakthrough preceding NO_2 as seen in Fig. 1A and B. Another striking difference on these samples is that the time for NOx breakthrough with H_2O in the lean feed (Figs. 2B and 3B) was longer than when H_2O and CO_2 were both absent (Figs. 2A and 3A). This is contradictory to the observation in Fig. 1A and B. These results imply that presence of water in the lean feed reduces the fast NSC of samples with 20%Ba and increases the fast NSC of the samples with 8%Ba and 4%Ba when compared to the fast NSC without CO_2 and H_2O in the feed on the respective samples. The same trends due to H_2O were observed on fast NSCs of the remaining samples with 20%Ba and 4%Ba (Fig. 5, compare series – 7%H_2O with series – neither H_2O nor CO_2) for which the breakthrough profiles are not shown. For 5.3Pt/4Ba, the sample with the highest Pt and lowest Ba loading was an exception, where fast NSC did not increase in presence of H_2O as compared to the fast NSC without CO_2 and H_2O in feed.

The fast NSC with CO_2 in lean feed on samples containing 20%Ba and 4%Ba increases linearly with Pt loading (Fig. 5). From E_{Pt} data in Table 2 we know that even though the fractions of exposed Pt on samples with 20%Ba are 30–40% lower than those on the 4%Ba samples, within each group of samples, those fractions are similar. Hence a threefold increase in Pt loading of two samples containing either 20%Ba or 4%Ba corresponds to approximately threefold increase in the absolute amount of exposed Pt present on them. In that case, the fast NSC on these samples, with CO_2 in the lean feed on the respective samples also increases threefold. This argument becomes clearer if we follow the fast NSC normalized by the absolute amounts of Ba on the samples, shown in Fig. 6. The fast NSC/Ba in presence of CO_2 for 0.7Pt/20Ba, 2.1Pt/20Ba and 6.3Pt/20Ba samples increased linearly with exposed Pt on those samples (Fig. 6). The same phenomenon was observed on 0.6Pt/4Ba, 1.9Pt/4Ba and 5.3Pt/4Ba under the same lean feed conditions (Fig. 6), although the absolute amount of fast NSC on 4%Ba samples was low, the error in its measurement was relatively high as compared to that for the 20%Ba samples. Surprisingly, fast NSC/Ba on 4%Ba samples under lean feed without CO_2 and H_2O also showed a linear increase with increase in exposed Pt (Fig. 6). In this case the absolute fast NSC on each 4%Ba sample was about three times that with CO_2 in lean feed (compare respective series in Fig. 5).

3.3. 'Fast' NOx storage with NO + O_2

Fig. 7 shows a steady-state NO oxidation simulation result on 2Pt/γ-Al_2O_3 monolith (E_{Pt} = 19%) with 300 ppm NO + 10%O_2 in Ar at 300 °C, 30,000 h^{-1} using NO oxidation kinetics from Mulla et al. [16]. It is clear from the NO and NO_2 concentration profiles that NO oxidation on Pt without NO_2 in the inlet feed, does not instantaneously convert the entire NO fed to NO_2. In the absence of a storage component like Ba, the monolith channel behaves as an integral reactor and NO_2 concentration builds up along the length

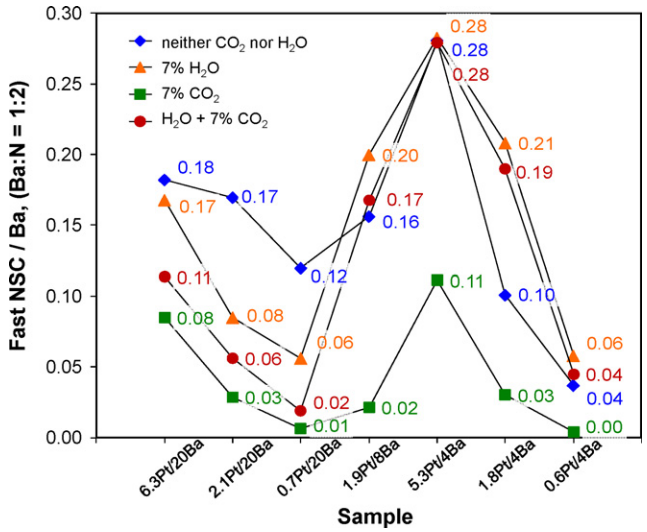

Fig. 6. Fast NOx storage capacity normalized with Ba (fast NSC/Ba) on sample (±0.01, using Ba:N = 1:2) at 300 °C, 30,000 h^{-1} with lean feed consisting of 300 ppm NO_2 + 10%O_2 + balance Ar and neither CO_2 nor H_2O, 7%H_2O, 7%CO_2, 7%H_2O + 7%CO_2.

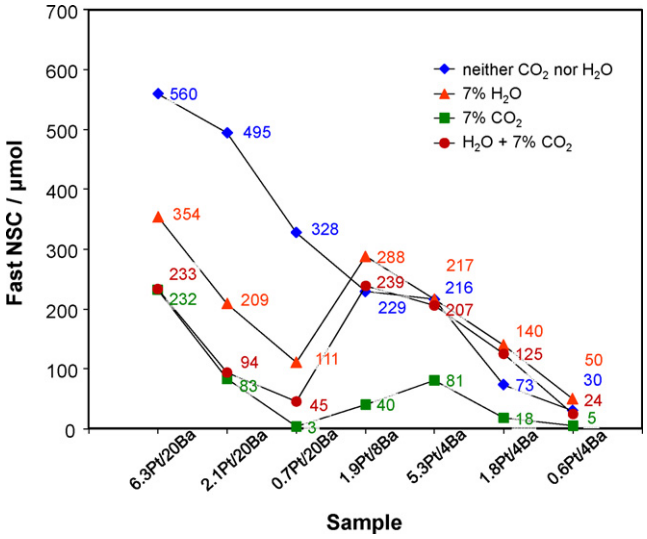

Fig. 8. Fast NOx storage capacity on sample (±10 µmol) at 300 °C, 30,000 h^{-1} with lean feed consisting of 300 ppm NO + 10%O_2 + balance Ar and neither CO_2 nor H_2O, 7%H_2O, 7%CO_2, 7%H_2O + 7%CO_2.

and inhibits the NO oxidation rate. Note that the local NO_2/NO ratio with the NO + O_2 feed in Fig. 7 is lower by more than an order of magnitude compared to the ratio at corresponding lengths (x/L) with the NO_2 + O_2 feed (Fig. 4). When Ba is present on the monolith, the NO_2 produced due to NO oxidation gets stored typically in the form of barium nitrates at 300 °C. We would observe a NO breakthrough as soon as the Pt/BaO/γ-Al_2O_3 LNT is exposed to lean feed conditions similar to those used in the simulation if NO_2 were the only species being stored during the fast NOx storage phase. This would lead to a zero fast NSC on LNTs with NO as the NOx source instead of NO_2 since the unconverted NO would escape the trap. Fast NSC measurements on the series of LNT samples we have studied are reported in Fig. 8. These measurements were obtained by applying the data analysis method described in Section 2.6 on data from experiments with lean feeds containing 300 ppm NO + 10%O_2 in Ar and (A) neither CO_2 nor H_2O, (B) 7%H_2O, (C) 7%CO_2, (D) 7%H_2O + 7%CO_2 at 300 °C, 30,000 h^{-1}. The non-zero fast NSCs with different lean feed compositions containing NO suggest that NO itself can directly be stored on Ba in addition to NO_2. This provides a basis for our hypothesis that there exists at least one NOx storage pathway without a preference between NO and NO_2 as a sorption precursor during fast NOx storage.

The data for fast NSC for the NO + O_2 feed normalized by the absolute amounts of Ba present on the sample, are reported in Fig. 9. Detailed analysis of the data in Figs. 8 and 9 makes it clear that the general trends due to effects of H_2O, CO_2 and H_2O + CO_2 on the fast NSC across the samples with NO as NOx source are the same as those with NO_2 as NOx source at the same temperature (300 °C) and GHSV (30,000 h^{-1}). Moreover, under the different lean feed compositions, *i.e.* with presence or absence of H_2O and CO_2, the absolute fast NSCs on all samples containing 8%Ba and 4%Ba with NO + O_2 (Fig. 8) were identical within the experimental measurement accuracy to those with NO_2 + O_2 (Fig. 5). This general observation concerning effect of NO vs. NO_2 in the lean feed on fast NSC of samples containing 8%Ba and 4%Ba did not hold true for samples containing 20%Ba. In the absence of CO_2 + H_2O, the comparison between fast NSC with NO_2 + O_2 (Fig. 5) vs. that with NO + O_2 (Fig. 8) on any 20%Ba sample containing the same exposed Pt shows that

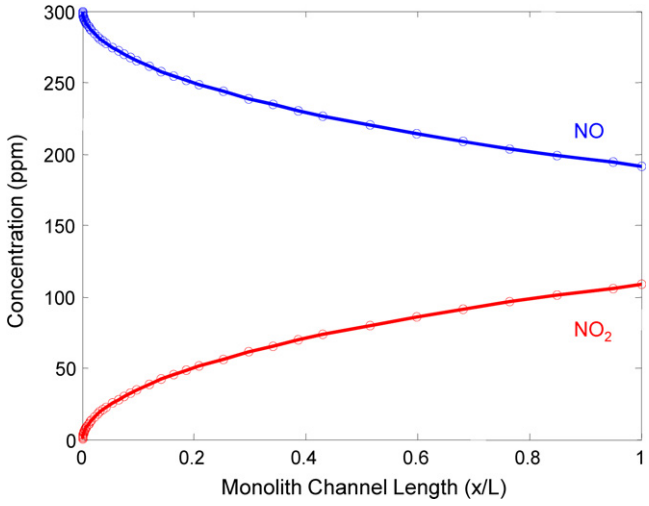

Fig. 7. Simulation result for steady-state NO oxidation, with 300 ppm NO + 10%O_2 + Ar on 2Pt/γ-Al_2O_3 (E_{Pt} = 19%) at 300 °C and 30,000 h^{-1}, leading to NO_2 buildup along the length of monolith channel.

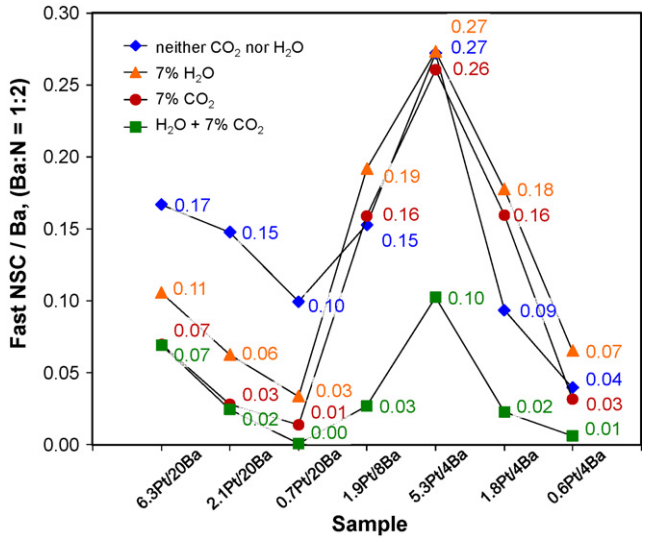

Fig. 9. Fast NOx storage capacity normalized with Ba (fast NSC/Ba) on sample (using Ba:N = 1:2) at 300 °C, 30,000 h^{-1} with lean feed consisting of 300 ppm NO + 10%O_2 + balance Ar and neither CO_2 nor H_2O, 7%H_2O, 7%CO_2, 7%H_2O + 7%CO_2.

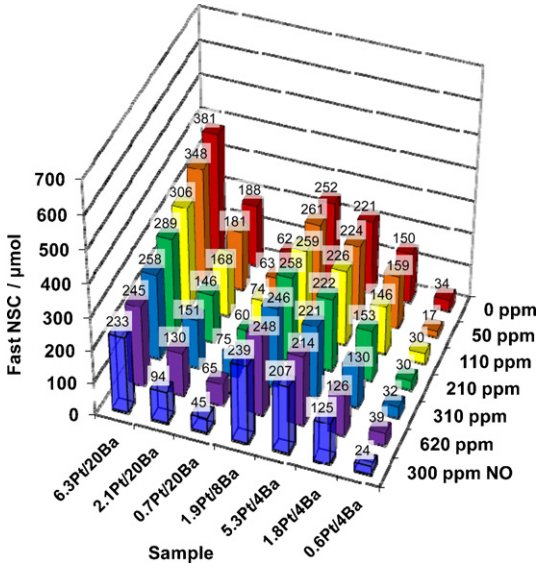

Fig. 10. Fast NOx storage capacity (±10 μmol) on LNT samples at 300 °C, 30,000 h^{-1} with lean feed consisting of 300 ppm NO_2 + 10%O_2 + *y* ppm NO + 7%CO_2 + 7%H_2O in Ar. For data series from back to front, *y* = 0, 50, 110, 210, 310 and 620 ppm, respectively. For comparison the front-most series shows NOx storage with lean feed of 300 ppm NO + 10%O_2 + 7%CO_2 + 7%H_2O in Ar.

the fast NSC decreased by 10–15% with NO + O_2 as the NOx source. In the presence of H_2O in feed the loss in fast NSC was between 27 and 40% and in presence of CO_2 + H_2O, it was in the range of 30–50% on these 20%Ba samples. The last lean feed composition, namely 300 ppm NO + 10%O_2 + 7%CO_2 + 7%H_2O in Ar is the most similar to that we would expect in a real lean automotive exhaust. It is worth noting that the largest drop in fast NSC with NO as the NOx source compared to NO_2 was observed for the most realistic feed composition on 20%Ba. In the presence of CO_2, the fast NSCs on the 20%Ba samples with NO_2 (Fig. 5) and NO (Fig. 8) as respective NOx sources were identical within the experimental measurement accuracy.

3.4. 'Fast' NOx storage with NO + NO_2 + O_2

To further examine the differences in responses of 20%Ba and 8%Ba, 4%Ba to NO and NO_2, we measured the fast NSC on all the samples in a set of experiments in which we used incremental amounts of NO in addition to 300 ppm NO_2 + 10%O_2 + 7%CO_2 + 7%H_2O in Ar in the lean feed to the monoliths at 300 °C, 30,000 h^{-1}. The results at these conditions are reported in Fig. 10. The rearmost series in Fig. 10 shows the fast NSC with 300 ppm NO_2 + 10%O_2 + 7%CO_2 + 7%H_2O in Ar. The effect of adding 50, 110, 210, 310 and 620 ppm NO to the base feed (rearmost series) is shown in the series of data from back to front except for the front-most series in Fig. 10, which shows the fast NSC with 300 ppm NO + 10%O_2 + 7%CO_2 + 7%H_2O in Ar. Note that in this data set we are increasing the NOx (NO_2 + NO) flux up to 3 times and causing up to an order of magnitude reduction in the inlet NO_2/NO ratio in the process of adding incremental amounts of NO to the base feed containing fixed amount of NO_2.

Fig. 10 shows that within ±10 μmol the absolute fast NSC on samples with 8%Ba and 4%Ba did not change due to incremental amounts of NO in the NO_2 + O_2 containing base feed as expected from the similarity of the responses of those samples to feeds containing NO_2 + O_2 (Fig. 5) and NO + O_2 (Fig. 8) as the NOx source. Since fast NSC, as given by the area of a rectangle as derived in Eq. (2) remained the same, the implication of this result is that time for 1% of the inlet NOx slip, t_{Sf}, was reduced by the same factor by which C^0_{NOx} was increased. The same phenomenon was observed on 0.7Pt/20Ba (Fig. 10). The 20%Ba samples with higher Pt loadings, *i.e.* 2.1Pt/20Ba and 6.3Pt/20Ba, clearly showed a decrease in fast NSC with a decrease in the inlet NO_2/NO ratio during these experiments. As the NO_2/NO ratio decreased, the fast NSC on these samples approached the values obtained with only NO + O_2 in the lean feed.

4. Discussion

Our definition of fast NSC given by Eq. (2) is purely functional and gives the maximum NOx storage capacity of the fully regenerated LNT before the NOx breakthrough begins. As will be discussed in detail below, the differences in the shapes of the breakthrough curves, immediately after the breakthrough, provide valuable insights into the fast NOx storage processes. The nature of these breakthrough curves and the dependence of t_{sf} on the operating variables on samples with 20%Ba vs. those with 8%Ba and 4%Ba, require that at least two NOx storage pathways involving at least as many types of Ba sites and time constants, as invoked in previous works from our laboratory [13,17], contribute to the fast NSC on Pt/BaO/γ-Al_2O_3 LNTs. It is also clear that in addition to the Ba loading, the fast NSC is also intricately linked with the Pt loading on the LNTs. Prior to the detailed discussion of a proposed mechanism of fast NOx storage, it is worthwhile to discuss the role of de-greening on the Pt, Ba morphology on our samples containing different Pt and Ba loadings.

4.1. Effect of de-greening on exposed Pt/Ba

As mentioned in Section 2.1, on our monolithic LNT samples, Pt was deposited on the γ-Al_2O_3 washcoat first, followed by Ba. In this scenario, it is safe to assume that the fractions of Pt exposed (E_{Pt}) on samples containing the same Pt loading (*e.g.* 2.1Pt/20Ba, 1.9Pt/8Ba and 1.8Pt/4Ba) were approximately the same prior to Ba deposition. Table 1 shows that after Ba deposition, the E_{Pt} decreased the least for 1.8Pt/4Ba (lowest Ba loading), decreased further for 1.9Pt/8Ba and decreased the most for 2.1Pt/20Ba (highest Ba loading) as compared to the identical E_{Pt} on these monoliths prior to Ba deposition. On a 200 m^2/g γ-Al_2O_3, similar to our samples, Yi et al. [63] have reported that loadings of 20%Ba, 8%Ba and 4%Ba correspond to 0.82, 0.29 and 0.14 monolayer (ML) of Ba, respectively. Under these circumstances, coverage of a large fraction of Pt by Ba explains the observed 25–30% lower E_{Pt} on fresh 2.1Pt/20Ba sample as compared to those on 1.9Pt/8Ba and 1.8Pt/4Ba samples. As the Ba coverage decreases, the probability of Pt being covered by Ba decreases resulting in correspondingly higher E_{Pt} (Table 1). The same argument applies to the rest of the samples. Using ultra-high-field solid-state MAS ^{27}Al-NMR, Kwak et al. [51] have shown that penta-coordinated Al^{3+} ions, the uniformly distributed surface defects on the γ-Al_2O_3, are the nucleation sites for BaO. They further claimed [52] that BaO monomers and dimers exist on the alumina surface at 4Ba and 8Ba loadings. At higher Ba loading, *i.e.* 20%Ba, Szanyi et al. [55] have reported the presence of large Ba crystallites (~60 nm) on freshly prepared 20Ba/γ-Al_2O_3 samples. These findings reported in the literature combined with trends in our E_{Pt} data on fresh samples (Table 1) lead us to conclude that 20%Ba samples are more likely to have large Ba particles, and significant coverage of Pt by Ba, while on the other hand, the Ba phase on 8%Ba and 4%Ba samples is highly dispersed with smaller Ba aggregates.

During the high-temperature (600 °C) step of the de-greening process, increase in Ba dispersion on 20%Ba samples leads to further coverage of Pt near large Ba particles resulting in as much as 7–16% reduction in E_{Pt} on 20%Ba samples after de-greening (Table 1). Using time resolved XRD studies, Szanyi et al. [55] have shown that Ba dispersion indeed increases on 20%Ba samples at as the temperature is

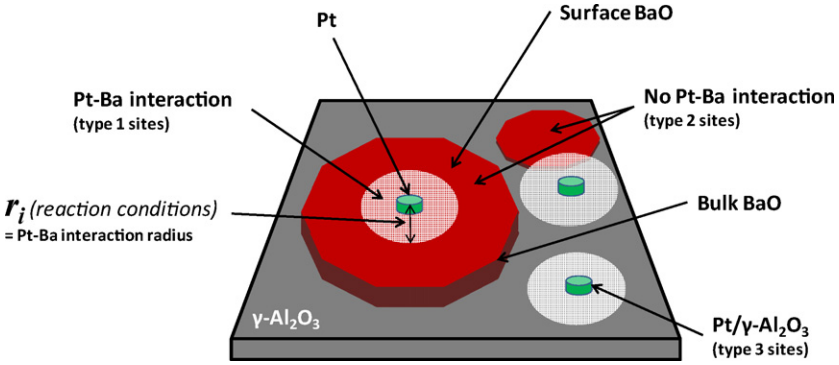

Fig. 11. Phenomenological model of Pt/BaO/γ-Al_2O_3 surface containing different types of Ba sites for 'fast' NOx storage on Pt/BaO/γ-Al_2O_3 with NO or NO_2 in lean feed at 300 °C.

increased above 550 °C. They also showed that subsequent cooling to room temperature and heating back to 300 °C under lean conditions did not change the Ba dispersion. We have already established that the Ba phase on 8%Ba and 4%Ba is highly dispersed even on the fresh samples; hence, we conclude that the 600 °C treatment did not have a large effect on those samples in terms of increasing the Ba dispersion which might cause the reduction in fraction of Pt exposed. The 4–6% drop in E_{Pt} on 8%Ba and 4%Ba samples (Table 1) is primarily caused by long exposure to H_2O at 300 °C, the low temperature de-greening step, as suggested by Mulla et al. [15] and Graham et al. [64] especially on samples with higher Pt loadings. We measured the fractions of Pt exposed after both 600 and 300 °C de-greening steps performed in random order (data not shown) to confirm our conclusions. The E_{Pt} reported in Table 1 is the final value after both steps were performed.

If the reactions during fast NOx storage on the entire amount of Ba on the sample were influenced by the amount of exposed Pt present, *e.g.* by catalysis of a specific NOx storage pathway by Pt, then the fast NSC of these samples would be proportional to the exposed Pt/Ba ratio (Table 2). A comparison between the trends in exposed Pt/Ba ratio (Table 2) and trends in fast NSC data from Fig. 6 with $NO_2 + O_2$ as the NOx source or Fig. 9 with $NO + O_2$ as the NOx source makes it clear that a simple proportionality relationship between fast NSC and exposed Pt/Ba ratio does not exist under all the feed conditions. One explanation is that the fast NSC on these samples is not proportional to the exposed Pt/Ba ratio because Pt affects only a fraction of the available Ba on the sample.

4.2. Phenomenological model for fast NOx storage

The concept, that the influence of Pt on Ba for NOx storage reactions might be localized around the Pt particle, has been used in the literature on different occasions to explain specific NOx storage data, as highlighted in Section 1. The explanation of the trends in our fast NSC data demands a model with parallel NOx storage pathways through which NOx can be stored on different types of Ba sites. Here, we start by proposing a phenomenological model based on the above mentioned concept of localized influence of Pt on Ba and parallel NOx storage reaction pathways on different Ba sites, and then we explain all the observed trends in our data presented in Section 3 based on the model and corresponding NOx storage reaction network in the discussion that follows.

Four types of sites (Fig. 11) which ultimately contribute to the measured fast NSC of LNTs under various feed conditions are as follows:

1. Ba vicinal to Pt (storage of NO_2 and/or NO using spilled over oxygen from Pt as the oxidant).
2. Ba uninfluenced by Pt (NO_2 disproportionation using NO_2 as the oxidant).
3. Pt/γ-Al_2O_3 (NO oxidation and NO_2 decomposition).
4. γ-Al_2O_3 (negligible NOx storage).

These sites support a complex reaction network which is described in Fig. 12.

This model allows the fast NSC to depend on how the Ba phase populates the area around the Pt particles. Moreover, parallel NOx storage reactions (Fig. 12) on Ba uninfluenced by Pt could also contribute to the fast NSC in addition to those on Ba vicinal to Pt. On samples with high Ba loading (*i.e.* 20%Ba), the region around Pt might be saturated by Ba and excess Ba would then be present in the region uninfluenced by Pt. On samples with lower Ba loading (*i.e.* 8%Ba and 4%Ba), the region around Pt might be under-populated by Ba leading to Pt-Ba/γ-Al_2O_3 and Ba/γ-Al_2O_3 sites which depend on Ba loading. On all the samples, local Pt/γ-Al_2O_3 and exposed γ-Al_2O_3 would also be available, the population of which would be a function of Pt, Ba loading and dispersion.

4.3. NOx storage on γ-Al_2O_3

A number of FT-IR, TPD and flow reactor studies on Pt/γ-Al_2O_3 and Pt/Ba/γ-Al_2O_3 have shown that NOx storage on γ-Al_2O_3 is typically negligible as compared to the amount stored on Ba at 300 °C [8,10,38,39]. If we consider our three samples with 4%Ba and different Pt loadings, where most of the alumina is exposed (≥86% [63]), the fast NSC without $CO_2 + H_2O$ in the feed shows a linear correlation with corresponding exposed Pt/Ba (Figs. 6 and 9, series A), implying that NOx storage on Ba vicinal to Pt is the major contributor to the fast NSC and not the NOx storage on γ-Al_2O_3. We have also observed that fast NSC increases with increasing Ba loading (and thus reducing exposed alumina) on 1.8Pt/4Ba, 1.9Pt/8Ba and 2.1Pt/20Ba (Figs. 6 and 9), even with a decreasing exposed Pt/Ba ratio (Table 2). This correlation corroborates the conclusion that storage on γ-Al_2O_3 is not a significant factor compared to the fast NSC on the Ba component of the LNTs. Furthermore, Toops et al. [65] have shown through their DRIFTS studies that in the presence of 5%H_2O, hydroxyl groups covered the alumina surface leading to reduction in NOx storage on alumina by as much as 92%. Thus, NOx storage on γ-Al_2O_3 would be even less important in the presence of water and is thus neglected from the discussion of fast NSC on our Pt/BaO/γ-Al_2O_3 LNTs.

4.4. Characteristics of the NO, NO_2 breakthrough profiles: fast NOx storage mechanism

With $NO_2 + O_2$ as the NOx source, on 20%Ba, without $CO_2 + H_2O$ (Fig. 1A) and with H_2O (Fig. 1B) in lean feed, NO_2 breakthrough fol-

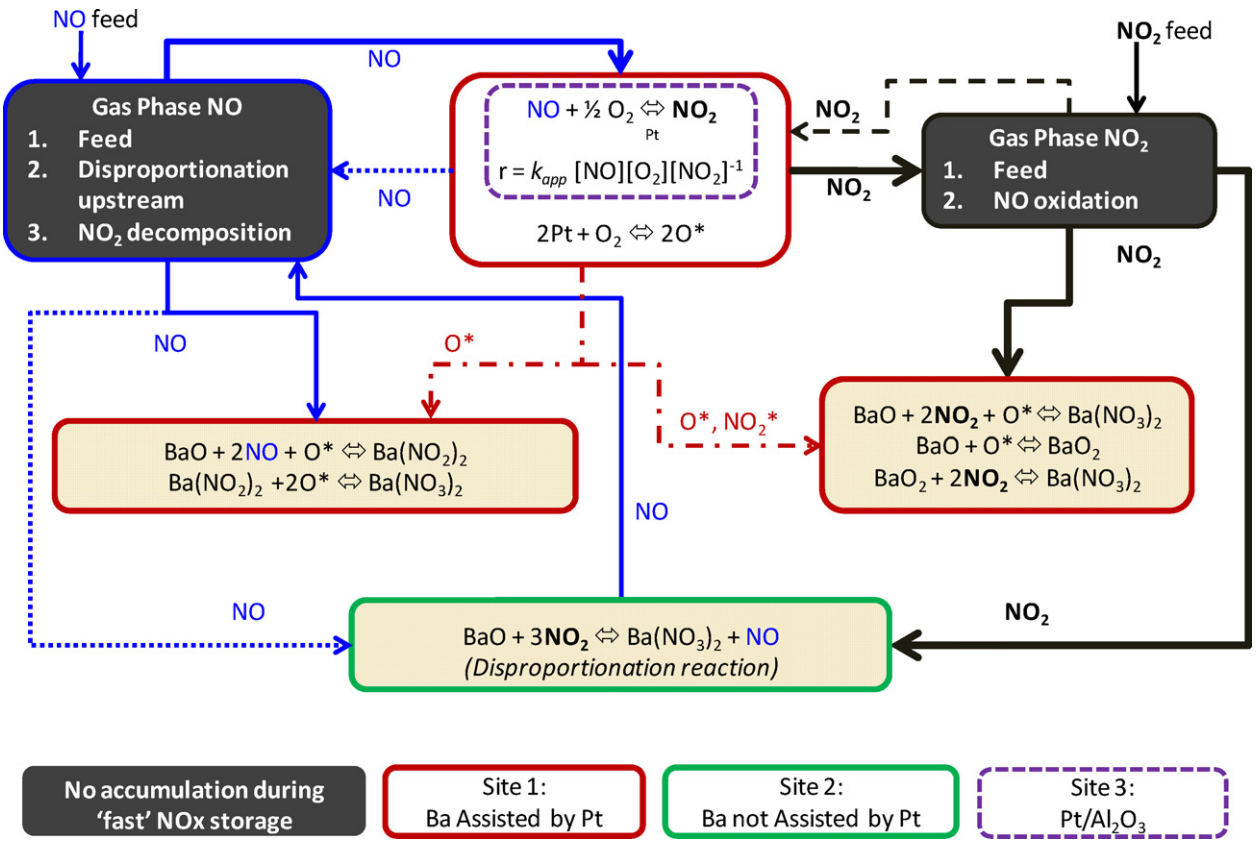

Fig. 12. Reaction network during fast NOx storage on Pt/BaO/γ-Al_2O_3 with NO or NO_2 in lean feed at 300 °C.

lows NO. The model accounts for these cases, by assuming that in addition to being stored on Ba vicinal to Pt using the spilled over oxygen as the oxidant to form $Ba(NO_3)_2$, some of the NO_2 is also being stored via the disproportionation pathway on Ba uninfluenced by Pt throughout the length of the monolith channel (Figs. 11 and 12). Therefore, NO breakthrough occurs as soon as the Ba sites vicinal to Pt saturate. Unlike NO_2, NO cannot be stored on Ba sites uninfluenced by Pt due to lack of an oxidant, resulting in NO_2 breakthrough lagging that of NO as it continues to store on Ba sites uninfluenced by Pt. Storage on the Ba sites vicinal to Pt is so fast that it occurs in a localized adsorption front and is limited by the supply of NO or NO_2 molecules. This adsorption front essentially titrates the Ba vicinal to Pt sites as it progresses along the monolith channel. With NO_2 as the sole NOx source, initially the front consists of NO_2 only, but as it progresses into the monolith channel, it contains a mixture of NO_2 and NO. The NO is produced during the comparatively slower process of NO_2 disproportionation on Ba sites uninfluenced by Pt and due to NO_2 decomposition (Fig. 4) upstream with respect to the adsorption front location. This NO is depleted by oxidation to NO_2 as it flows downstream over Pt (Fig. 7), leading to its storage on Ba sites downstream, but this pathway alone cannot possibly account for disappearance of the entire amount of NO since all of it is not oxidized to NO_2 instantaneously (Fig. 7). Direct adsorption of NO on Ba vicinal to Pt, using spilled over oxygen atoms as the oxidant, accounts for the disappearance of rest of the NO at 300 °C. NO adsorbed on Pt is likely to be converted to NO_2 which then travels to Ba vicinal to Pt by surface diffusion or it can desorb and readsorb downstream on Ba uninfluenced by Pt. NO could also be adsorbed on Ba species vicinal to Pt forming an intermediate, which can then convert to stable $Ba(NO_3)_2$ using a spilled over oxygen from Pt if that process occurs within the lifetime of the intermediate species at 300 °C.

Interestingly, in the presence of H_2O on samples with 8%Ba and 4%Ba, the NO and NO_2 breakthroughs are simultaneous (Fig. 2B) or NO slightly lags behind NO_2 (Figs. 2D and 3B and D). This result is consistent with the model if we assume that on these samples the ratio of Ba sites uninfluenced by Pt to the Ba sites vicinal to Pt is small vs. that on 20%Ba sample. Thus, fast NOx storage via NO_2 disproportionation is not significant on samples with lower loading with highly dispersed Ba and high exposed Pt/Ba ratio (Table 2). NO_2 decomposition on Pt upstream of the adsorption front is then the primary source of NO. NO thus produced is consumed downstream mainly by direct adsorption on Ba vicinal to Pt and only a small fraction might get re-oxidized to NO_2 over Pt. This scenario would lead to simultaneous NO_2 and NO breakthrough or NO_2 breakthrough followed by NO as observed. This result is also consistent with our claim that NOx essentially titrates the Ba vicinal to Pt sites.

With CO_2 in the lean feed on 20%Ba (Fig. 1C) the shape of NO_2 and NO breakthrough has a noticeably lower slope while rising to the inlet NOx level, as compared to the cases without CO_2 and H_2O (Fig. 1A) and with H_2O (Fig. 1B) and the time for NOx breakthrough (t_{sf}) is shorter by 3–6 times, respectively. At 300 °C, with CO_2 in the lean feed, barium carbonates or carboxylates are present on the trap, depending on the Ba loading [32,57]. A simultaneous NO and NO_2 breakthrough implies that the replacement of these carbonate/carboxylate groups by $Ba(NO_3)_2$ formation via the NO_2 disproportionation mechanism on Ba uninfluenced by Pt is slow. It is slow enough that within the time required to saturate the Ba vicinal to Pt through the parallel oxygen spillover mechanism its contribution to the fast NSC of the LNT is negligible. Hence we conclude that presence of CO_2 in the lean feed substantially reduced the effective population of Ba uninfluenced by Pt, available for fast NOx storage on 20%Ba.

On 20%Ba samples, fast NSC with $CO_2 + H_2O$ (Figs. 1D and 5) in the feed takes an intermediate value between those with CO_2

(Fig. 5) and H_2O (Fig. 5, see respective series) which implies that kinetics of hydroxyl group replacement with nitrates must be faster than kinetics of carbonate/carboxylate replacement as both barium carbonates/carboxylates and hydroxides are known to coexist on Ba at these conditions [32]. Thus, the chemical phase to which Ba is converted during the regeneration step prior to NOx storage due to the presence of CO_2 and/or H_2O, plays a key role in governing the fast NSC on these LNTs. Similar to the trend observed on 20%Ba, 8%Ba and 4%Ba samples also show that the fast NSC with $CO_2 + H_2O$ (Figs. 2D, 3D, and 5) takes an intermediate value between that with CO_2 and that with H_2O. The full effects of H_2O and CO_2 on fast NSC are discussed in detail in the following sections.

4.5. Role of Pt, Ba in the presence of H_2O

The presence of H_2O in the feed appears to have reduced the effective population of Ba vicinal to Pt on 20%Ba, as the time for breakthrough (t_{sf}) is half (Fig. 1B) of that measured when CO_2 and H_2O were both absent in the lean feed (Fig. 1A). Contrary to this behavior, on samples with 8%Ba (Fig. 2A vs. B) and 4%Ba (Fig. 3A vs. B) the presence of H_2O appears to have enhanced the effective population of Ba vicinal to Pt as t_{sf} increased in the presence of H_2O. Fast NSC with NO_2 or NO as the NOx source, in presence of H_2O in feed, shows this peculiar trend for all 20%Ba vs. 8%Ba and 4%Ba samples (compare respective series within Figs. 5 and 8). Our DRIFTS results [66] also corroborate the ability of H_2O to block NOx storage on 20%Ba. For example, at 300 °C, on the 2.1Pt/20Ba sample, the ionic/bulk nitrate peak intensity was significantly lower in the presence of H_2O in the feed as compared to the case without H_2O and CO_2 in the feed. On the other hand, on 1.9Pt/8Ba and 1.8Pt/4Ba, the ionic/bulk nitrate peak intensity increased with a simultaneous decrease in bidentate/surface nitrate peak intensity with H_2O in the feed, as compared to the spectra for the case without H_2O and CO_2 in the feed on respective samples. This is also consistent with the trends in fast NSC on 8%Ba and 4%Ba samples reported in this work.

The reversible morphology change in the Ba phase during fast NOx storage from surface Ba (highly dispersed) to larger Ba agglomerates (bulk like) due to the presence of H_2O, suggested also by Szanyi et al. [56], explains the reduction of fast NSC on 20%Ba, as loss in surface Ba sites uninfluenced by Pt would lead to further reduction in the contribution to fast NSC by NO_2 disproportionation pathway. The agglomeration of Ba might also uncover some of the Pt particles leading to an increase in population of Ba vicinal to Pt. This increased Pt–Ba vicinal site population explains the increase in fast NSC with increasing Pt loading on 20%Ba samples (Figs. 5 and 8, series—7%H_2O).

The argument for loss of surface Ba due to agglomeration in presence of H_2O on 20%Ba samples fails to explain the trends seen on 8%Ba and 4%Ba samples (Figs. 5 and 8). On these samples, smaller and highly dispersed Ba clusters exist compared to those on 20%Ba. Szanyi et al. [56] have reported that on 8%Ba samples on exposure to lean feed containing NO_2, the NSC remains the same in absence and presence of H_2O but the all the surface nitrates in the former case were converted to ionic/bulk nitrates in presence of H_2O at 27 °C. They also note that this process is strongly temperature and H_2O pressure dependent. As noted earlier, our DRIFTS results [66] on 8%Ba and 4%Ba samples, at 300 °C, also show partial conversion of surface nitrates to ionic/bulk nitrates in presence of H_2O. At short exposure times, these DRIFTS-based results on 8%Ba and 4%Ba samples showing Ba agglomeration and fast NSC data from flow reactor experiments showing an increase in fast NSC in presence of H_2O, lead us to postulate that the rate of NO_2 disproportionation is Ba cluster size sensitive, such that it increases as very small Ba clusters grow to a certain size and after that the rate levels off. *In situ* Ba particle size and NO_2 disproportionation reaction kinetics measurements under relevant conditions would be required in order to experimentally verify the postulate.

Interestingly, on 8%Ba and all the 4%Ba samples with different Pt loadings, the fast NSC without CO_2 and H_2O in feed (Figs. 5 and 8) remains the same within analytical accuracy (±10 μmol) for both NO_2 and NO as the NOx source and in both cases, the fast NSC follows the same linear relation with exposed Pt/Ba ratio (Figs. 6 and 9, Table 2). A linear relationship with exposed Pt implies that only the NOx storage on Ba vicinal to Pt contributes to the fast NSC. Thus, on these 8%Ba and 4%Ba samples, the increase in the fast NSC in presence of H_2O is in accordance to our postulate regarding the dependence of NO_2 disproportionation reaction rate on Ba cluster size as Ba morphology is the only variable that changed in presence of H_2O with fraction of Pt exposed being the same on each of these samples. The increase in fast NSC in presence of H_2O, on 8%Ba and 4%Ba samples (Figs. 5 and 8) with increasing exposed Pt/Ba ratio (Table 2) is attributed to the increase in the population of Ba vicinal to Pt sites due to increase in number of Pt particles.

4.6. Role of Pt, Ba in the presence of CO_2

On all the samples, at 300 °C, in presence of CO_2, the fast NSC decreased drastically with both NO_2 and NO as the NOx source as compared to respective cases without CO_2 or H_2O in lean feed (compare series – neither CO_2 nor H_2O with series – 7%CO_2 within Figs. 5 and 8). Furthermore, in the presence of CO_2, the fast NSC increases linearly with exposed Pt/Ba ratio (Table 2) on all samples with 20%Ba, 8%Ba and 4%Ba. This result is extremely important in this discussion. The dynamics of replacement of carbonate and carboxylate species on Ba by NO or NO_2 in presence of CO_2 in the feed is driven by a competition between the rate of formation of barium nitrate and the rate of formation of the carbonate/carboxylate species. The linear dependence of fast NSC on exposed Pt/Ba ratio provides a sound basis for the hypothesis that the intermediates formed on Ba uninfluenced by Pt during carbonate/carboxylate replacement do not get oxygen fast enough to be converted into the thermodynamically stable $Ba(NO_3)_2$ species at 300 °C. Hence, in the presence of CO_2 in the lean feed, carbonate/carboxylate species on Ba uninfluenced by Pt are difficult for NOx to replace even at 300 °C. On the other hand, on Ba vicinal to Pt, $Ba(NO_3)_2$ species are formed much faster by utilizing spilled over oxygen adatoms from Pt to oxidize the intermediate. Therefore, only the NO_2 and NO storage on Ba vicinal to Pt contributes to fast NSC on all 20%Ba, 8%Ba and 4%Ba monoliths in presence of CO_2 in lean feed at 300 °C. Furthermore, the reduction in fast NSC on 8%Ba and 4%Ba samples in with CO_2 in the feed, with NO and NO_2 as the NOx source, compared to that without CO_2 and H_2O in the feed (compare series – neither CO_2 nor H_2O with series – 7%CO_2 within Figs. 5 and 8) implies that presence of CO_2 reduces the effective population of Ba sites vicinal to Pt. On 20%Ba samples, the difference in fast NSC is driven by both the decrease in effective population of Ba sites vicinal to Pt and the loss of the contribution from NOx storage on Ba sites uninfluenced by Pt in the presence of CO_2 in the feed.

The fast NSC value in the presence of $CO_2 + H_2O$ in lean feed falls between the fast NSC with H_2O (upper limit) and with CO_2 (lower limit) for each respective sample. This phenomenon can be caused by competing effects of H_2O and CO_2 on fast NOx storage, discussed in this section and in Section 4.5.

4.7. Effect of NO on fast NOx storage

As seen in Fig. 7, the NO oxidation simulation shows that on Pt/γ-Al_2O_3 at 300 °C, for NO + O_2 as the feed, the NO_2 concentration slowly builds up along the length of the monolith channel leading to an increase in the local NO_2/NO ratio. In that case, Ba at the inlet of the monolith channels does not take part in NOx storage since

sufficient NO_2 is not present for adsorption [18]. This is referred to as the 'inlet effect'. The loss in fast NSC during NOx storage with NO as the NOx source instead of NO_2 as the NOx source was observed only on our LNT samples with the highest Ba loading (*i.e.* 20%Ba) and not on those containing 8%Ba and 4%Ba (Figs. 5 and 8). From results in Fig. 10, it is clear that fast NSC is lost only on 20%Ba samples even with the mixed NOx source containing $NO + NO_2$.

These results can be explained with our model as follows. As concluded in Section 4.4, the NOx breakthrough occurs as soon as the Ba sites vicinal to Pt are saturated. When we measure fast NSC as described by Eq. (2), we essentially measure the amounts of NOx stored through parallel storage pathways (Fig. 12) on both types of Ba sites until the Ba sites vicinal to Pt are saturated. Based on the analysis of the nature of NOx breakthrough curves (Section 4.4), our hypothesis is that the fast NOx storage on Ba vicinal to Pt is a NO/NO_2 supply limited process without a preference between NO and NO_2 as the NOx source. It is clearly seen on 8%Ba and 4%Ba samples (Fig. 10) that as NOx flux is increased, it requires proportionally less time for the population of Ba vicinal to Pt to saturate leading to identical fast NSCs.

On the 20%Ba samples, the contribution of storage by NO_2 disproportionation is a significant fraction of the fast NSC when NO_2 is the NOx source. As the NOx flux is increased by increasing NO (thus reducing inlet $NO_2/NO \leq 6$), the Ba vicinal to Pt saturates in proportionally less amount of time since there is no preference between NO and NO_2 as the NOx source on those sites. At the same time fast NSC is lost due to the lower contribution to NOx storage via NO_2 disproportionation within allowed time for NOx breakthrough, which is governed by the time required to saturate the Ba vicinal to Pt sites. As NO_2 is the preferred species for adsorption via NO_2 disproportionation on Ba uninfluenced by Pt, when NO is used as a NOx source, since it does not get converted into NO_2 instantaneously on entering the monolith channel (Fig. 7), the disproportionation pathway is not efficiently utilized along the length of the monolith channel where NO_2/NO is low, especially near the inlet of the monolith channel. As a result within the time for NOx breakthrough the amount of NOx stored on Ba uninfluenced by Pt is lower with NO as the NOx source, rather than NO_2. Thus, the kinetically dominant pathway of NO and NO_2 adsorption on Ba vicinal to Pt governs the fast NOx storage process and hence the loss of fast NSC on 20%Ba samples with NO as the NOx source instead of NO_2. For the 8%Ba and 4%Ba samples, all the fast NOx storage occurs on Ba vicinal to Pt. Therefore, there is no difference between fast NSC with NO_2 or NO as the NOx source and no inlet effect.

5. Conclusions

The fast NOx storage capacity (fast NSC) of the fully regenerated $Pt/BaO/\gamma\text{-}Al_2O_3$ LNTs, with various Pt and Ba loading combinations was studied. This fast NSC is the maximum amount of NOx the trap can store before the NOx breakthrough occurs. This aspect of the LNT operation is what makes their application commercially important. All the LNT samples were studied under lean feed compositions consisting of combinations of NO, NO_2, CO_2 and H_2O at 300 °C, 30,000 h^{-1}. Their fast NSC under different lean feed conditions was evaluated according to our functional definition of fast NOx storage (Eq. (2)) and detailed analysis of the NOx breakthrough profiles was performed. In order to explain different aspects of the entire set of experimental results presented in Section 3, a phenomenological model for LNT surface morphology and accompanying reaction network for fast NOx storage process were proposed. The model consists of four types of sites due to various Pt, Ba loading conditions (Figs. 11). They are as follows:

1. Ba vicinal to Pt (storage of NO_2 and/or NO using spilled over oxygen from Pt as the oxidant).
2. Ba uninfluenced by Pt (NO_2 disproportionation using NO_2 as the oxidant).
3. $Pt/\gamma\text{-}Al_2O_3$ (NO oxidation and NO_2 decomposition).
4. $\gamma\text{-}Al_2O_3$ (negligible NOx storage).

These sites support a network of series and parallel reaction pathways as presented in Fig. 12.

With the assistance of results published in the literature and using our results as the experimental evidence, it was suggested that fast NSC of $\gamma\text{-}Al_2O_3$ is negligible at 300 °C. It was shown that at 300 °C, Ba sites vicinal to Pt have dominant contribution to the fast NSC on samples with Ba weight loadings ranging from 20 to 4 wt.%, with either NO or NO_2 as the NOx source and also in the presence of CO_2 and/or H_2O in the lean phase feed. Platinum plays a significant role in fast NOx storage process through the coupling with proximal Ba sites by spilled over oxygen atoms which are necessary to form the thermodynamically stable $Ba(NO_3)_2$ species at the temperature studied, from both NO_2 or NO as the NOx source.

Through the analysis of NOx breakthrough profiles under different lean feed compositions and steady-state NO oxidation simulations on $Pt/\gamma\text{-}Al_2O_3$, it was hypothesized that there is no preference between NO and NO_2 as a precursor for adsorption on Ba sites vicinal to Pt, irrespective of the Ba loading. It was also concluded that the adsorption on these sites occurs at a localized adsorption front. The Ba sites vicinal to Pt get titrated by the front consisting of NO and NO_2 as it moves through the length of the monolith channel. NOx adsorption on these sites is limited by the supply of NO and/or NO_2 molecules. It was also shown, across the studied Pt and Ba loading range, that in the presence of NO as the NOx source or with an $NO + NO_2$ mixture with low inlet NO_2/NO ratio ($\leq$6) as the NOx source, NOx storage on Ba vicinal to Pt is dominant over storage due to NO_2 disproportionation and that the dynamics of the former process controls the time for NOx breakthrough and thus the fast NSC.

It was found that NO_2 disproportionation on Ba uninfluenced by Pt has negligible contribution to fast NSC on these LNTs in presence of CO_2 in the lean feed mixture, irrespective of the Ba loading. The absolute fast NSCs of all the samples in presence of CO_2 were singularly dependent on the amount of exposed Pt on the respective sample. The oxygen availability for Ba vicinal to Pt drives this phenomenon at 300 °C as it can assist in the formation of thermodynamically stable $Ba(NO_3)_2$ as carbonate/carboxylate groups are displaced within the time allowed before NOx breakthrough begins.

In the presence of H_2O, the fast NSCs on 20%Ba were negatively affected while those on the 8%Ba and 4%Ba samples were enhanced as compared to fast NSCs on the respective samples without CO_2 and H_2O in lean feed. From the FT-IR studies of Szanyi et al. [56,67] and DRIFTS results from our laboratory [66], it is known that the Ba phase reversibly agglomerates in presence of H_2O in the feed at the reaction conditions used in this work. We attribute the decrease in fast NSC in the presence of H_2O to the loss of surface Ba uninfluenced by Pt sites on 20%Ba. While, on samples with 8%Ba and 4%Ba where Ba phase is highly dispersed and exists in the form of small Ba clusters, Ba agglomeration in presence of H_2O leads to increased contribution to fast NSC from NOx storage via NO_2 disproportionation reaction which is only active on larger Ba clusters. From the presented results, it is clear that in the presence of CO_2 and H_2O in the feed, the fast NSC primarily depends on the nature of the initial state of the Ba phase on the surface and that the hydroxyl groups are more easily replaced than carbonate/carboxylates on Ba sites vicinal to Pt. In the presence of $CO_2 + H_2O$ in the feed, the fast NSC values are between those in presence of CO_2 (lower limit) and those in presence of H_2O (upper limit). This can be attributed to mixed effects due to CO_2 and H_2O as discussed above.

These results have direct impact on modeling of the NOx storage phase of the NOx Storage Reduction cycles under various feed conditions and for different Pt, Ba loadings. The insights can also be utilized in the design of LNT formulations using optimum amounts of Pt, based on required operating condition constraints.

Acknowledgements

The authors thank the Indiana 21st Century Research and Technology Fund and Cummins Inc. for financial support of this work. We thank Dr. Hai-Ying Chen and Dr. Howard Hess of Johnson Matthey Catalysts for preparing and providing us with the specific set of catalyst samples used in this study. We also thank Dr. Shadab Mulla, Dr. Joshua Ratts, Dr. Lei Cao and Dr. Yuri Zvinevich for many productive and enlightening discussions regarding various aspects of this work.

References

[1] W.S. Epling, L.E. Campbell, A. Yezerets, N.W. Currier, J.E. Parks, Catal. Rev. Sci. Eng. 46 (2004) 163.
[2] M.V. Twigg, Appl. Catal. B 70 (2007) 2.
[3] M. Takeuchi, S.i. Matsumoto, Top. Catal. 28 (2004) 151.
[4] N. Takahashi, H. Shinjoh, T. Iijima, T. Suzuki, K. Yamazaki, K. Yokota, H. Suzuki, N. Miyoshi, S.-i. Matsumoto, et al., Catal. Today 27 (1996) 63.
[5] W. Bogner, M. kramer, B. Krutzsch, S. Pischinger, D. Voigtlander, G. Wenninger, F. Wirbeleit, M.S. Brogan, R.J. Brisley, D.E. Webster, Appl. Catal. B 7 (1995) 153.
[6] P.T. Fanson, M.R. Horton, W.N. Delgass, J. Lauterbach, Appl. Catal. B 46 (2003) 393.
[7] J.H. Kwak, D.H. Kim, T. Szailer, C.H.F. Peden, J. Szanyi, Catal. Lett. 111 (2006) 119.
[8] B. Westerberg, E. Fridell, J. Mol. Catal. A: Chem. 165 (2001) 249.
[9] F. Prinetto, G. Ghiotti, I. Nova, L. Castoldi, L. Lietti, E. Tronconi, P. Forzatti, Phys. Chem. Chem. Phys. 5 (2003) 4428.
[10] F. Prinetto, G. Ghiotti, I. Nova, L. Lietti, E. Tronconi, P. Forzatti, J. Phys. Chem. B 105 (2001) 12732.
[11] L. Cumaranatunge, S.S. Mulla, A. Yezerets, N.W. Currier, W.N. Delgass, F.H. Ribeiro, J. Catal. 246 (2007) 29.
[12] S.S. Mulla, S.S. Chaugule, A. Yezerets, N.W. Currier, W.N. Delgass, F.H. Ribeiro, Catal. Today 136 (2008) 136.
[13] L. Cao, J.L. Ratts, A. Yezerets, N.W. Currier, J.M. Caruthers, F.H. Ribeiro, W.N. Delgass, Ind. Eng. Chem. Res. 47 (2008) 9006.
[14] S.S. Mulla, N. Chen, L. Cumaranatunge, G.E. Blau, D.Y. Zemlyanov, W.N. Delgass, W.S. Epling, F.H. Ribeiro, J. Catal. 241 (2006) 389.
[15] S.S. Mulla, N. Chen, L. Cumaranatunge, W.N. Delgass, W.S. Epling, F.H. Ribeiro, Catal. Today 114 (2006) 57.
[16] S.S. Mulla, N. Chen, W.N. Delgass, W.S. Epling, F.H. Ribeiro, Catal. Lett. 100 (2005) 267.
[17] B.R. Kromer, L. Cao, L. Cumaranatunge, S.S. Mulla, J.L. Ratts, A. Yezerets, N.W. Currier, F.H. Ribeiro, W.N. Delgass, J.M. Caruthers, Catal. Today 136 (2008) 93.
[18] M. Al-Harbi, W.S. Epling, Catal. Lett. 130 (2009) 121.
[19] R.D. Clayton, M.P. Harold, V. Balakotaiah, C.Z. Wan, Appl. Catal. B: Environ. 90 (2009) 662.
[20] J.A. Anderson, B. Bachiller-Baeza, M. Fernandez-Garcia, Phys. Chem. Chem. Phys. 5 (2003) 4418.
[21] J.A. Anderson, A.J. Paterson, M. Fernandez-Garcia, Stud. Surf. Sci. Catal. 130B (2000) 1331.
[22] N.W. Cant, I.O.Y. Liu, M.J. Patterson, J. Catal. 243 (2006) 309.
[23] N.W. Cant, M.J. Patterson, Catal. Today 73 (2002) 271.
[24] W.S. Epling, J.E. Parks, G.C. Campbell, A. Yezerets, N.W. Currier, L.E. Campbell, Catal. Today 96 (2004) 21.
[25] S. Erkfeldt, E. Jobson, M. Larsson, Top. Catal. 16/17 (2001) 127.
[26] S. Hodjati, C. Petit, V. Pitchon, A. Kiennemann, Appl. Catal. B 27 (2000) 117.
[27] S. Hodjati, K. Vaezzadeh, C. Petit, V. Pitchon, A. Kiennemann, Catal. Today 59 (2000) 323.
[28] K.S. Kabin, P. Khanna, R.L. Muncrief, V. Medhekar, M.P. Harold, Catal. Today 114 (2006) 72.
[29] O. Monticelli, R. Loenders, P.A. Jacobs, J.A. Martens, Appl. Catal. B 21 (1999) 215.
[30] F. Rodrigues, L. Juste, C. Potvin, J.F. Tempere, G. Blanchard, G. Djega-Mariadassou, Catal. Lett. 72 (2001) 59.
[31] E. Fridell, M. Skoglundh, B. Westerberg, S. Johansson, G. Smedler, J. Catal. 183 (1999) 196.
[32] L. Lietti, P. Forzatti, I. Nova, E. Tronconi, J. Catal. 204 (2001) 175.
[33] W.S. Epling, G.C. Campbell, J.E. Parks, Catal. Lett. 90 (2003) 45.
[34] H. Mahzoul, J.F. Brilhac, P. Gilot, Appl. Catal. B 20 (1999) 47.
[35] X. Li, M. Meng, P. Lin, Y. Fu, T. Hu, Y. Xie, J. Zhang, Top. Catal. 22 (2003) 111.
[36] Y. Li, S. Roth, J. Dettling, T. Beutel, Top. Catal. 16/17 (2001) 139.
[37] E. Fridell, H. Persson, B. Westerberg, L. Olsson, M. Skoglundh, Catal. Lett. 66 (2000) 71.
[38] R.D. Clayton, M.P. Harold, V. Balakotaiah, AIChE J. 55 (2009) 687.
[39] A. Lindholm, N.W. Currier, E. Fridell, A. Yezerets, L. Olsson, Appl. Catal. B 75 (2007) 78.
[40] J. Szanyi, J.H. Kwak, D.H. Kim, S.D. Burton, C.H.F. Peden, J. Phys. Chem. B 109 (2005) 27.
[41] T. Kobayashi, T. Yamada, K. Kayano, SAE Tech. Paper 970745, 1997.
[42] I. Nova, L. Castoldi, F. Prinetto, V. Dal Santo, L. Lietti, E. Tronconi, P. Forzatti, G. Ghiotti, R. Psaro, S. Recchia, Top. Catal. 30/31 (2004) 181.
[43] I. Nova, L. Castoldi, L. Lietti, E. Tronconi, P. Forzatti, F. Prinetto, G. Ghiotti, J. Catal. 222 (2004) 377.
[44] P. Gambardella, Z. Sljivancanin, B. Hammer, M. Blanc, K. Kuhnke, K. Kern, Phys. Rev. Lett. 87 (2001) 056103/1.
[45] I. Nova, L. Lietti, L. Castoldi, E. Tronconi, P. Forzatti, J. Catal. 239 (2006) 244.
[46] R. Buchel, R. Strobel, F. Krumeich, A. Baiker, S.E. Pratsinis, J. Catal. 261 (2009) 201.
[47] J. Despres, M. Koebel, O. Krocher, M. Elsener, A. Wokaun, Appl. Catal. B 43 (2003) 389.
[48] L. Olsson, R.J. Blint, E. Fridell, Ind. Eng. Chem. Res. 44 (2005) 3021.
[49] L. Olsson, D. Monroe, R.J. Blint, Ind. Eng. Chem. Res. 45 (2006) 8883.
[50] U. Tuttlies, V. Schmeisser, G. Eigenberger, Top. Catal. 30/31 (2004) 187.
[51] J.H. Kwak, J.Z. Hu, D.H. Kim, J. Szanyi, C.H.F. Peden, J. Catal. 251 (2007) 189.
[52] J.H. Kwak, D. Mei, C.-W. Yi, D.H. Kim, C.H.F. Peden, L.F. Allard, J. Szanyi, J. Catal. 261 (2009) 17.
[53] A. Lindholm, N.W. Currier, J. Dawody, A. Hidayat, J. Li, A. Yezerets, L. Olsson, Appl. Catal. B 88 (2009) 240.
[54] E.C. Corbos, X. Courtois, F. Can, P. Marécot, D. Duprez, Appl. Catal. B 84 (2008) 514.
[55] J. Szanyi, J.H. Kwak, J. Hanson, C. Wang, T. Szailer, C.H.F. Peden, J. Phys. Chem. B 109 (2005) 7339.
[56] J. Szanyi, J.H. Kwak, D.H. Kim, X. Wang, R. Chimentao, J. Hanson, W.S. Epling, C.H.F. Peden, J. Phys. Chem. C 111 (2007) 4678.
[57] I. Nova, L. Castoldi, L. Lietti, E. Tronconi, P. Forzatti, Catal. Today 75 (2002) 431.
[58] K.M. Adams, G.W. Graham, Appl. Catal. B 80 (2008) 343.
[59] W.S. Epling, D. Kisinger, C. Everest, Catal. Today 136 (2008) 156.
[60] J.E. Benson, M. Boudart, J. Catal. 4 (1965) 704.
[61] M.A. Vannice, Kinetics of Catalytic Reactions, Springer, 2005.
[62] L. Cumaranatunge, Ph.D. Thesis, Purdue University (2006).
[63] C.W. Yi, J.H. Kwak, C.H.F. Peden, C. Wang, J. Szanyi, J. Phys. Chem. C 111 (2007) 14942.
[64] G.W. Graham, H.W. Jen, W. Chun, H.P. Sun, X.Q. Pan, R.W. McCabe, Catal. Lett. 93 (2004) 129.
[65] T.J. Toops, D.B. Smith, W.S. Epling, J.E. Parks, W.P. Partridge, Appl. Catal. B 58 (2005) 255.
[66] S.S. Chaugule, V. Kispersky, J.L. Ratts, W.N. Delgass, F.H. Ribeiro, unpublished results.
[67] J. Szanyi, J.H. Kwak, R.J. Chimentao, C.H.F. Peden, J. Phys. Chem. C 111 (2007) 2661.